A Comparison of Two- and Three-Dimensional Wave Breaking

H. M. NEPF AND C. H. WU

Department of Civil and Environmental Engineering, Massachusetts Institute of Technology, Cambridge, Massachusetts

E. S. CHAN

Department of Civil Engineering, National University of Singapore, Singapore

(Manuscript received 24 January 1997, in final form 8 October 1997)

ABSTRACT

The influence of directionality on wave-packet evolution and in particular on the onset of breaking was explored through laboratory experiment. Lateral tapering was applied to the input signal to produce a range of crest lengths, with greater directionality created by diffraction for the shorter crests. The wave shape, local and global wave steepness, and surface displacement spectra were used to characterize the wave fields. The observations suggest that directionality can accelerate or suppress the onset of breaking, and additionally can influence both the local wave steepness at breaking as well as the breaking severity. Directionality, however, did not alter the observed up-frequency energy transfer associated with wave focusing. When no breaking occurred this energy shift was completely reversed. With breaking the shifted energy was lost, that is, passed from the wave to the turbulent energy field. The short-crested wave packet lost 16% of its energy as a result of breaking, while a comparable two-dimensional breaker lost 22%.

1. Introduction

Oceanic wave breaking provides an important conduit for the exchange of gas, water vapor, energy, and momentum between the atmosphere and the ocean (Melville 1996). These exchanges affect the growth of wind waves (Phillips 1977), the generation of bubbles and sea spray (Johnson and Cooke 1979; Thorpe 1993), the formation of surface currents (Longuet-Higgins 1969; Mitsuyasu 1985; Melville and Rapp 1988; Rapp and Melville 1990), and the generation and distribution of near-surface turbulence (Koga 1982; Blanchard and Woodcock 1980; Gargett 1989; Thorpe 1995). Recent studies have also shown that breaking waves may retard global warming by increasing CO_2 fluxes to the ocean (Bryan and Spelman 1985; Csanady 1990). In addition, the forces associated with freak wave breaking threaten both offshore structures and ships (Kjeldsen and Myrhaug 1994; Chan and Melville 1988; Greenhow and Vinje 1982). In view of the many important consequences of wave breaking, it is crucial to have a fundamental understanding of this process and, in particular, to have the ability to predict the onset of breaking events and their severity in terms of energy loss.

Over a century ago theorists began to examine the limits of wave stability. Using a breaking criteria based on the crest particle velocity exceeding the phase speed, the breaking limit of the two-dimensional Stokes wave was shown to occur at a wave steepness, $ak = 0.443$, and crest angle 120°, where a is wave amplitude and k is wavenumber (Stokes 1880; Michell 1893; Havelock 1918). However, theoretical and experimental results have since shown that finite amplitude Stokes waves, given sufficient fetch, are unstable at much lower steepness due to the growth of two forms of instability, longitudinal (Type I) and lateral (Type II) modulation (Benjamin and Feir 1967; McLean 1982; Longuet-Higgins 1985a). For an initial steepness $a_0k_0 > 0.25$ the evolution of lateral modulation can lead to three-dimensional spilling breakers (Melville 1982; Su 1982; Su et al. 1982).

A variety of other wave forms have been examined experimentally. For example, steady waves created by towed hydrofoils have a breaking onset of $H/L = 0.10$, where H and L are the local wave height and length, respectively (Duncan 1981, 1983). Assuming a symmetric wave, this steepness value is roughly equivalent to $ak = 0.31$. In contrast, for quasi-steady breakers generated between convergent walls the observed onset criteria was $H/L = 0.132$, or $ak = 0.41$ (Ramberg and Griffin 1987). The difference in these results suggests that a breaking onset criteria based on local wave steepness is sensitive to the process of wave generation.

Field and laboratory studies have shown that, as a

Corresponding author address: Dr. H. M. Nepf, Department of Civil and Environmental Engineering, Massachusetts Institute of Technology, Room 48-425, Cambridge, MA 02139.
E-mail: hmnepf@mit.edu

wave approaches breaking, the wave profile becomes both horizontally and vertically asymmetric, and so deviates from the symmetric profile of the theoretical wave shape (Kjeldsen and Myrhaug 1979; Bonmarin 1989; Tulin and Li 1992). Most notably the front of the crest becomes steeper than the rear, reflecting an intrawave energy shift; that is, the energy of the crest and front simultaneously increase at the expense of the trough and back (Bonmarin 1989; Tulin and Li 1992). The local steepness ak, while appropriate for the theoretical, symmetric wave, is inappropriate for the characterization of real waves because it cannot reflect this profile asymmetry. To capture the asymmetry a new wave-shape parameter was introduced, the front-crest steepness, ε (Kjeldsen and Myrhaug 1979). Unfortunately, the new steepness parameter was only marginally better than ak in terms of providing a stable breaking criteria (Kjeldsen and Myrhaug 1979). Indeed, the range of limiting steepness observed in the field, $\varepsilon = [0.32 \text{ to } 0.78]$, suggests that this single point characterization of local wave shape is not capable of discerning the physical limits of breaking.

Rapp and Melville (1990) considered a global spectrum-based steepness, ak_c, to describe the breaking onset for two-dimensional, unsteady breakers generated through wave–wave interaction within frequency-modulated wave packets. Here, a is the sum of the component amplitudes a_n, and k_c the wavenumber of the center frequency. For a top-hat spectrum, that is, constant component amplitude, the onset of breaking was observed at $ak_c = 0.25$. In addition, ak_c was shown to have reasonable correlation to breaker severity as measured by fractional energy loss, which ranged from 10% for spilling breakers up to 25% for plunging breakers. Using the same wave generation technique, Chaplin (1996) compared two different spectral forms, a constant component amplitude and a constant component steepness, and found different onset criteria $ak_c = 0.265$ and 0.30, respectively, indicating that the breaking onset criteria based on ak_c are sensitive to spectral shape.

Theorists and field investigators have also considered breaking criteria based on the downward acceleration at the crest (Penney and Price 1952; Taylor 1953; Phillips 1958). For the almost highest wave, Longuet-Higgins (1986) has shown that the Eulerian (apparent) acceleration in the crest tends to infinity, but that the Lagrangian (real) acceleration is limited to $-0.388g$. To apply these results to the field one must consider the affect of unsteadiness. Longuet-Higgins (1985b) suggested that unsteady waves may be considered as the superposition of steady, progressive waves of differing frequency. The constructive interference leads to higher accelerations at the crest for lower overall steepness, suggesting that unsteady waves break at lower overall steepness than do steady waves. This result, however, does not consider the effect of wave-field directionality.

As a simplification for directional wave fields, She et al. (1994) and Kolaini and Tulin (1995) specifically explored the influence of spatial focusing. Both studies demonstrated that, as the angle of wave interaction increased (0° corresponding to a planar wave front), both the breaking height and the breaking severity also increased. Interestingly, this trend is counter to that suggested for the superposition of unidirectional, multifrequency progressive waves, described above. However, the observed increase in breaking steepness with focusing angle is consistent with Penney and Price (1952), who used a limiting acceleration criteria to predict that the breaking steepness of a standing wave, that is, maximum focusing angle, exceeds that of a progressive wave by 50%. Taylor (1953) verified this prediction qualitatively in a laboratory tank, but suggested that three-dimensional modulation, which appeared as the predicted limiting wave height was approached, assisted in the precipitation of breaking.

Field observations, which correlated photographic images of whitecapping to vertical acceleration within a directional wave field, support a breaking criteria of $-0.5g$ (Snyder et al. 1983). In contrast, other investigations of random, deep-water wave fields have suggested threshold values of $-0.39g$ (Ochi and Tsai 1983), $-0.34g$ (Dawson et al. 1993), and $-0.32g$ (Longuet-Higgins 1985b). The discrepancy between these different observations may be attributed to differences in Eulerian and Lagrangian observational methods, as well as to the influence of multiple frequency superposition and directionality on real crest acceleration.

The experiments described in this paper were intended to build on several of the above studies by further examining the details of breaking within a directional wave field. The study provides a direct comparison of the evolution and breaking criteria for spectrally similar two- and three-dimensional wave packets created through frequency focusing. To contrast the directional focusing explored by She et al.(1994) and Kolaini and Tulin (1995), this study explored the influence of passive directional spreading (diffraction), and demonstrates that both the local breaking steepness (§3a) as well as the breaking severity (§3d) are diminished under conditions of diffraction. This is complementary to previous observations of increasing breaking steepness and severity with increasing wave focusing (She et al. 1994; Kolaini and Tulin 1995). In addition, the limiting spectrum-based steepness increased with increasing diffraction, suggesting that breaking may be suppressed in a strongly diverging field (§3b). Directionality, however, did not influence the up-frequency shift in wave energy associated with the approach to breaking (§3c).

2. Experimental methods

a. Wave generation

The present study was conducted in a 4 m × 11 m test section within the Gunther Family Wave Basin at the Massachusetts Institute of Technology. The mean

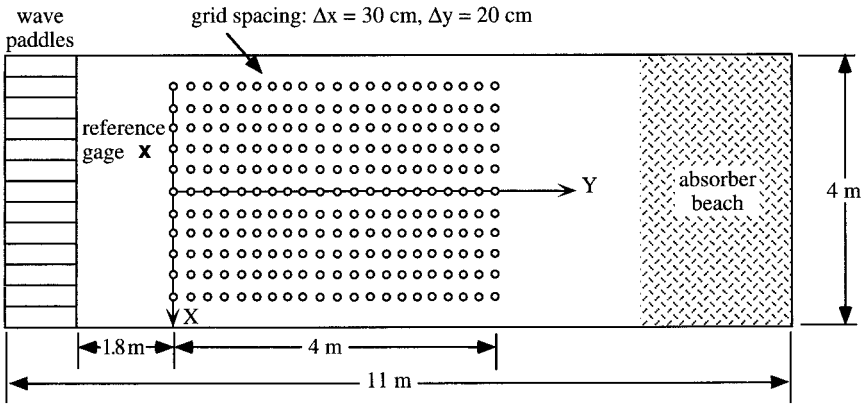

FIG. 1. Top view of test section. Circles indicate the locations of surface displacement measurements. To verify repeatability and to synchronize different runs a reference gauge was maintained at $y = -20$ cm, $x = -30$ cm.

water depth was $h = 0.6$ m. The waves were generated using 13 independently programmed and hydraulically driven paddles, each 30 cm wide. A coordinate system was chosen with y as the longitudinal direction and $y = 0$ at the first measurement position; x as the lateral direction and $x = 0$ at the midpoint of the test section, $z = 0$ at the mean water level and positive upward. The breaking events occurred within a 4 m $\times$ 4 m measurement area (Fig. 1), which began 180 cm (=3 h) from the mean position of the paddles to avoid interference from the evanescent modes associated with the paddles (Dean and Dalrymple 1984).

A single, unsteady breaker can be generated using frequency focusing. This technique, based on the constructive interference of dispersive wave components, was first used by Cummins (1962) and Davis and Zarnick (1964) for testing ship models. Greenhow and Vinje (1982) and Rapp and Melville (1990) have also used this technique to generate individual, isolated breakers within a wave packet. The technique mimics the wave–wave interaction, which is believed to be the fundamental process producing unsteady breaking in the field (Tulin and Li 1992). It is important to note, however, that other mechanisms such as wave–current interaction (Kjeldsen and Myrhaug 1980), direct wind forcing (Banner and Phillips 1974), and fetch (Su and Green 1985) may also affect the breaking processes. Here, we followed the frequency focusing technique described in Rapp and Melville (1990) but applied a different distribution of component amplitudes a_n, and limited the lateral extent of the wave packet to achieve a short-crested breaker.

To begin, linear wave theory was used to derive the surface displacement required at the paddles, $\eta(y_p, t)$, in order to produce constructive interference and breaking at a prescribed distance y_b measured from the mean position of the paddles:

$$\eta(y_p, t) = \sum_{n=1}^{N} a_n \cos[-k_n y_b - 2\pi f_n(t - t_b)], \quad (1)$$

where t_b is the theoretical time of breaking (maximum focusing), and a_n and f_n are the amplitude and frequency for each of N wave components. Because the wave becomes nonlinear in its approach to breaking, (1) is not strictly valid near the prescribed focal point and the actual point of breaking may occur later than, that is, downstream of, the theoretical value (Baldock et al. 1996). The wavenumber of each component k_n is given by the linear dispersion relation

$$(\omega_n)^2 = k_n g \tanh(k_n h), \quad (2)$$

where g is the gravitational constant, and the radian frequency, $\omega_n = 2\pi f_n$. The surface displacement may then be described by the variables N, a_n, f_n, y_b, t_b, and k_n, defined for each paddle, and the global parameters h and g. These variables can be reduced to a shorter set of dimensionless parameters as follows.

The spectrum parameters were chosen to produce a specific spectral shape that mimics the high-frequency tail of the wind wave spectrum, f^{-5} (Phillips 1958). The number of wave components N was chosen at 32 in order to approximate a continuous spectrum. The 32 components, f_n, were equispaced across a bandwidth of Δf and centered at frequency f_c. The component amplitudes were then chosen to produce a constant wave steepness for all wave components; that is,

$$a_n = G/k_n, \quad (3)$$

where G is a scale factor (Loewen and Melville 1991). In contrast to a constant component amplitude, that is, $a_n = \text{const}$, this condition inhibits premature breaking because all components maintain similar scale with regard to steepness.

The intensity of the wave packet can be described in terms of a global, spectrum-based wave steepness, ak_c, defined by Rapp and Melville (1990),

$$ak_c = k_c \sum_{n=1}^{32} a_n, \quad (4)$$

where a_n was defined by (3). The wavenumber of the

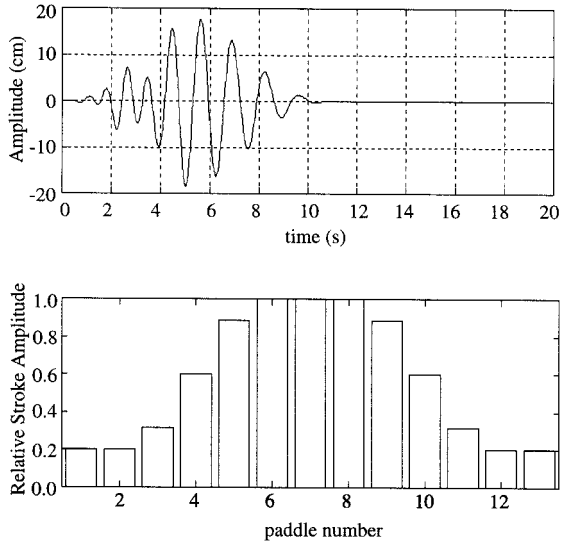

FIG. 2. Input signal of centerline wave paddle (a). To create a short-crested wave packet the centerline signal is tapered to 20% using a cosine window. An example of the taper function is shown in (b).

central frequency k_c is given by f_c and (2). With spectral shape held constant, ak_c was varied through the scale factor G.

To produce a two-dimensional wave, the input signal (1) was identically defined for each of the 13 paddles. To introduce directionality, a limited crest length was created by spatially tapering the individual paddle movements. The central paddles moved together at the maximum amplitude (Fig. 2a) and the remaining paddles were tapered down to 20% using a cosine window (Fig. 2b). This spatial variation mimics field conditions in which local heterogeneity within the wind field produces local heterogeneity within the wave field. By varying the number of central paddles the forced crest length, L_0, was varied from 30 to 150 cm. For the two-dimensional breaker L_0 was effectively infinite. The transverse tapering produced passive directional spreading during wave evolution. The extent of directional defocusing (diffraction) was dependent on both the initial crest length and the distance to breaking, yielding a dimensionless diffraction parameter, y_b/L_0.

The three-dimensional wave packet evolution can now be described by the nondimensional set: (ak_c, y_b/L_0, $\Delta f/f_c$, k_ch). Varied conditions of ak_c and y_b/L_0 were considered in this study. The frequency bandwidth ratio, $\Delta f/f_c$, has been shown to have only a weak influence on breaker onset and severity (Rapp and Melville 1990, Fig. 17), and so was not varied here. A fixed value of $\Delta f/f_c = 0.73$ ($\Delta f = 0.789$ Hz and $f_c = 1.08$ Hz) was selected because it produced the most distinct transition between the spilling and plunging cases (Rapp and Melville 1990). Finally, we considered deep water waves such that the last parameter, k_ch, had little effect on the wave evolution. From the wavenumber $k_c = 4.73$ m^{-1}, $\tanh(k_ch) = 0.99$, indicating a deep water wave condition at the scale of the wave packet.

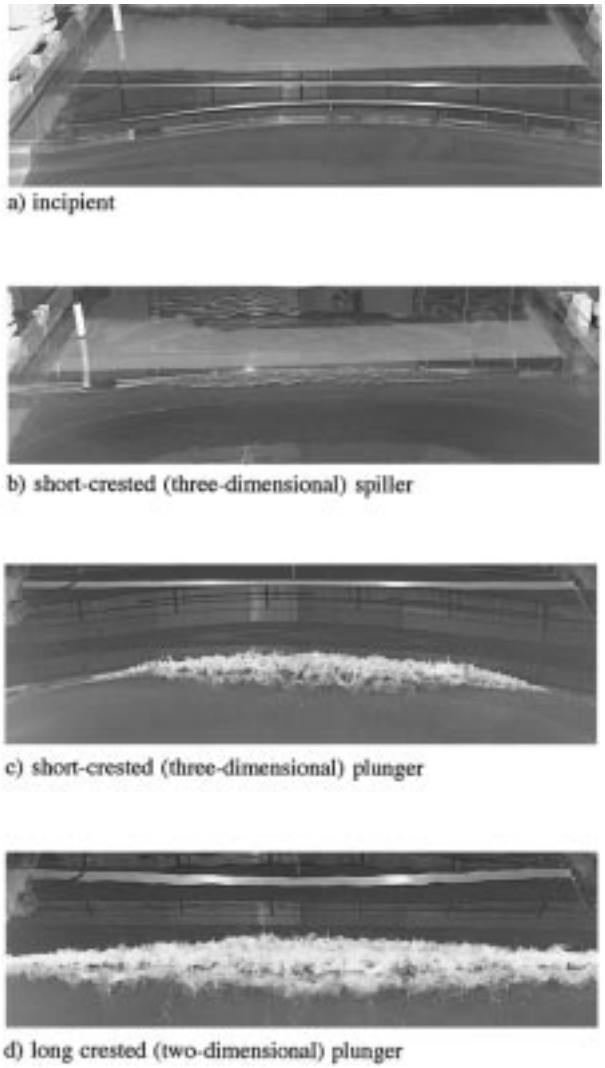

FIG. 3. Photograph of the breaking crest taken from above and behind the wave, that is, the crest is moving away from the camera: (a) three-dimensional incipient wave crest, (b) three-dimensional spilling wave crest, (c) three-dimensional plunging crest, and (d) two-dimensional plunging crest.

The limiting conditions for nonbreaking, spilling, and plunging waves were determined as follows. Starting with a nonbreaking wave, the gain was slowly increased for successive runs, producing a nonbreaking, spilling, and finally a plunging wave. The wave was classified as nonbreaking if the free surface remained visually smooth throughout the run (Fig. 3a). The largest steepness at which a nonbreaking wave was observed was defined as the incipient breaking criteria. At larger values of ak_c a slight spilling began at $y_b = 420$ cm, manifest in a ruffled surface appearance along the central wave crest (Fig. 3b). Increasing ak_c further eventually produced a second breaker at $y_b = 300$ cm, that is,

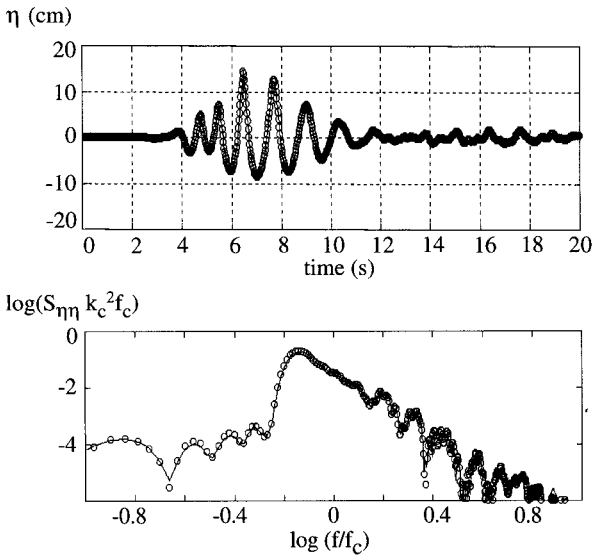

FIG. 4. (a: top) The records of surface elevation measured at the reference gauge are compared for run number 5 (open circles), corresponding to the gauge array positioned at $y = 80$ cm, and run number 12 (solid line), corresponding to the gauge array positioned at $y = 180$ cm. The records demonstrate the excellent repeatability of the wave-packet conditions. (b: bottom) The spectra of the records shown in (a). The total energy of the individual wave packets agree to within 1%.

upstream of the original spiller. The onset of this upstream wave was chosen as the spilling criteria as it represents the strongest individual spiller that could be produced within the wave packet. Finally, ak_c was increased to the point at which the upstream breaker became a plunger (Fig. 3c), and the downstream spiller disappeared. This condition represented the weakest plunger that could exist alone, that is without a secondary breaker downstream. The two-dimensional plunger (Fig. 3d) was similarly selected, but with uniform paddle forcing ($y_b/L_0 = 0$).

b. Free surface displacement

The surface displacement was recorded for 40 seconds at 40 Hz using 4-mm diameter, resistance-type wave gauges. Wave records were measured at 126 grid positions spaced 30 cm in the lateral (x) direction, and 20 cm in the longitudinal (y) direction (see Fig. 1). A tighter spacing was chosen for Δy to capture the more rapid spatial variation. A carriage system holding six wave gauges was used to traverse the measurement grid. Allowing for symmetry across the centerline, the entire test section could be scanned using 21 runs. Between each run the basin was required to settle for 15 minutes to eliminate all previous surface motion.

Before each testing session the following measurements were made to verify the experimental conditions and to minimize error. First, the wave gauges were calibrated and the accuracy, ± 0.2 mm, confirmed. Second,

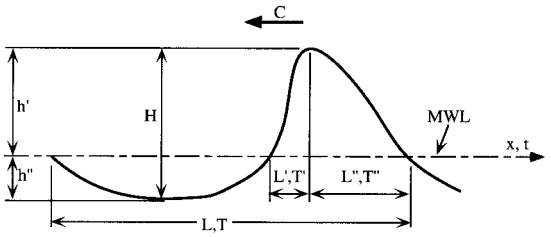

FIG. 5. A definition sketch for the determination of crest-front steepness, $\varepsilon = \eta'/L' = (2\pi\eta')/(gTT')$, where T is the observed wave period, and T' is the time interval associated with the passage of the front crest region defined as the interval between the passage of the crest-front zero crossing and the wave peak. Taken from She et al. (1994)

pairs of surface elevation records, $\eta(t)$, measured at symmetric positions on either side of centerline were compared to verify the centerline symmetry. The mean-square deviation between records at several longitudinal positions matched to within 1%–2%, confirming symmetry. Third, to test the repeatability of wave generation and to synchronize the multiple wave records, a stationary reference wave gauge was maintained at the position ($y = -20$ cm, $x = -30$ cm). For any two runs the surface displacement record at the reference gauge were essentially indistinguishable (e.g., Fig. 4a). In addition, the spectra and the total spectral energy observed at the reference gauge agreed between any two runs to within 1% (Fig. 4b). Finally, the influence of beach reflection was evaluated for steady waves at the central frequency by comparing wave records at three gauges unevenly spaced along the channel (Rosengaus-Moshinsky 1987). Extrapolating these results to the wave packet, we determined that reflection contributed less than 5% error to the estimation of local wave-packet energy.

c. Wave shape parameters

Two wave shape parameters were considered. First, the wave steepness ak_c was used to characterize the potential steepness of a wave within a modulated wave packet based on the steepness of the spectral components. It represents a global estimate of the wave steepness and was evaluated from (3) and (4) above. Second, a local wave steepness was estimated using the temporal records of surface displacement at each wave gauge. To capture crest asymmetry, the front crest steepness was chosen to represent the local wave shape (Kjeldsen and Myrhaug 1979; Bonmarin 1989). The crest front steepness, $\varepsilon = \eta'/L'$, was evaluated as

$$\varepsilon = \frac{2\pi\eta'}{gTT'}, \tag{5}$$

where η', L', T, and T' are defined in Fig. 5.

d. Spectral analysis

At each measurement position the surface displacement spectra $S_{\eta\eta}$ was calculated for the wave packet, which was isolated from the extended record by a tapered window. Zero padding was applied to extend the record for a 4096 point FFT with a 256 point smoothing filter. The resulting spectra were used to evaluate the intrawave harmonic exchange associated with changes in wave shape, in particular the increasing steepness and asymmetry observed as the wave focuses and approaches breaking. To more clearly evaluate these changes, the spectrum was divided into two frequency bands. The principle frequency band, 0.7–1.5 Hz, corresponded to the input signal. Upshifted energy was observed in a second band of frequencies, 1.5–3.0 Hz. The energy content of each frequency band, E_1 and E_2, was estimated by integrating the spectrum over the corresponding frequency range. Changes in E_1 and E_2 were used to interpret cross-frequency exchanges of energy, as well as diffraction effects.

e. Energy fluxes

As the wave packet propagated downstream changes in local wave-packet energy arose from diffraction, viscous dissipation in the wall- and bottom-boundary layers, and breaking. Diffraction, resulting from the lateral variation in wave energy, contributes a net loss (or gain) only within a longitudinal slice of limited lateral extent. If the entire basin width is considered, then diffraction merely redistributes wave energy, contributing no net loss from the width-averaged wave packet. Thus, to eliminate diffraction from the energy budget, we chose a control volume that spans the basin width, $-b/2 < x < b/2$; is bound from below by the basin bottom, $z = -h$; is bound from above by the free surface, $z = \eta$; and finally is bound by the longitudinal positions of $y_1 = 0$ and $y_2 = 4.0$ m. This control volume roughly corresponds to the measurement grid points shown in Fig. 1. Using laterally averaged quantities, we write the following conservation equation (Mei 1983):

$$\frac{\partial E}{\partial t} + \frac{\partial F}{\partial y} = -\rho \overline{\int_{z=-h}^{\eta} (e + e_b)\, dz}, \tag{6}$$

where e is the rate of viscous dissipation within the sidewall and bottom boundary layers, and e_b is the rate of energy loss due to breaking, both per unit volume, and ρ is the fluid density. The overbar represents a time average over the wave-packet interval, t_1 to t_2, where t_1 occurs before the arrival of and t_2 occurs after the departure of the wave packet. The laterally averaged energy density E and energy flux F are defined by

$$E = \int_{x=-2m}^{x=+2m} \overline{\int_{z=-h}^{\eta} \rho\left(\frac{1}{2}(u^2 + v^2 + w^2) + gz\right) dz}\, dx \tag{7}$$

$$F = \int_{x=-2m}^{x=+2m} \overline{\int_{z=-h}^{\eta} \left(p + \frac{1}{2}\rho(u^2 + v^2 + w^2) + \rho g z\right) v\, dz}\, dx \tag{8}$$

with the velocity field (u, v, w) corresponding to the directions (x, y, z), respectively. The analysis is completed by integrating over the control volume length, y_1 to y_2:

$$\int_{y_1}^{y_2} \frac{\partial E}{\partial t}\, dy + \int_{y_1}^{y_2} \frac{\partial F}{\partial t}\, dy = -\int_{y_1}^{y_2} \rho \int_{x=-2m}^{x=+2m} \overline{\int_{-h}^{\eta} (e + e_b)\, dz}\, dx\, dy$$

$$\Delta F = [e]_T + [e_b]_T. \tag{9}$$

If we assume that all mean currents and turbulence generated by the breaking are contained within the control volume, then the motions at y_1 and y_2 are purely wave. Then, at t_1 (before the arrival of the packet) and at t_2 (after the packet has passed by) the wave energy, $E = 0$ at both y_1 and y_2, and the first term in (9) is zero. This assumption is supported by observations of dye tracer injected into the water column and observed with an underwater camera. The tracer indicated that mean currents initiated by the breaking event were contained between y_1 and y_2 during the time t_1 to t_2. The second term in (9) is the net difference in total wave energy flux at the longitudinal boundaries of the control volume, for simplicity ΔF. The third term is the net loss of energy from the wave packet due to both viscous dissipation $[e]_T$ and breaking $[e_b]_T$.

The evaluation of (9) requires detailed temporal and spatial measurement of the velocity and pressure fields in addition to the surface displacement. However, reasonable flux estimates may be made using surface displacement only. The second-order estimate of the energy flux associated with the wave motion is given by $F = C_g E$. If the wave motion at y_1 and y_2 is at most weakly nonlinear then an equi-partition of potential and kinetic energy may be assumed and the local energy density may be given as $E = \rho g \overline{\eta^2}$, where $\overline{\eta^2}$ is the surface displacement variance. To construct comparative flux estimates along the channel using $\overline{\eta^2}$ alone we must additionally assume that the group velocity C_g is constant along the channel. This assumption, however, is not strictly true, as surface displacement records indicated a 12%–18% downshift in phase velocity after breaking, similar to observations made by Bonmarin (1989) for two-dimensional waves. A smaller change in

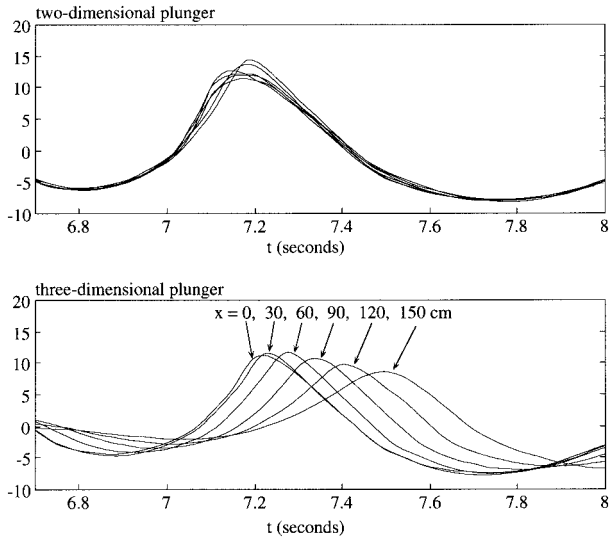

FIG. 6a. The two-dimensional plunger breaks evenly across the channel, with all lateral positions observing a plunging breaker. In contrast the three-dimensional plunger breaks in a crescent shape, with the centerline leading. In addition, the three-dimensional crest is a composite of breaking intensity. At $x = 0$, 30, and 60 cm the wave is plunging; at $x = 90$ cm the wave is spilling; $x = 120$ cm marks the edge of the breaking regions; and the wave is not breaking at $x = 150$.

group velocity is expected, however, as only the central crest was downshifted.

Finally, normalizing by values at the upstream position $y_1 = 0$ m, denoted by subscript "0," the fractional change in wave energy flux may be given as

$$\Delta F/F_0 = \Delta(\overline{\eta^2})/\overline{\eta_0^2}, \tag{10}$$

remembering that the terms in (10) represent cross-sectional averages based on the measurements from 11 lateral grid positions. While (10) is not generally valid close to the point of breaking because the assumptions of energy equipartition and constant group velocity fail there, previous experiments have shown that (10) does provide a reasonable estimate of flux variation at positions up- and downstream of the breaking point. (Rapp and Melville 1990).

3. Results

a. Breaking criteria based on local wave steepness

With an initial crest length, $L_0 = 90$ cm, the three-dimensional wave packet produced a crescent-shaped breaking crest 220 cm in length, that is, limited to less than one-half the channel width. The two-dimensional wave packet produced a spatially uniform crest that

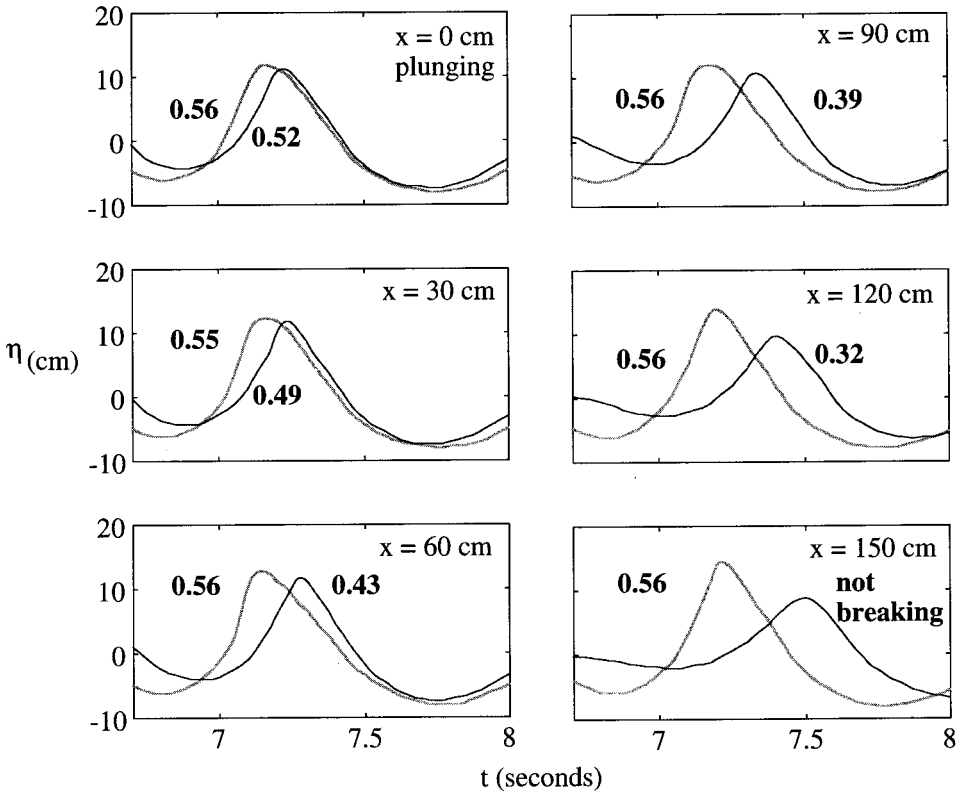

FIG. 6b. Comparison of wave shape at onset of breaking. The black line corresponds to the three-dimensional wave crest and the gray line to the two-dimensional wave crest. The lateral position x of record is given in the upper right of each figure. The values of limiting front-crest steepness are given in bold numerals. By visual inspection the edge of the breaking region for the short-crested wave is $x = 120$ cm.

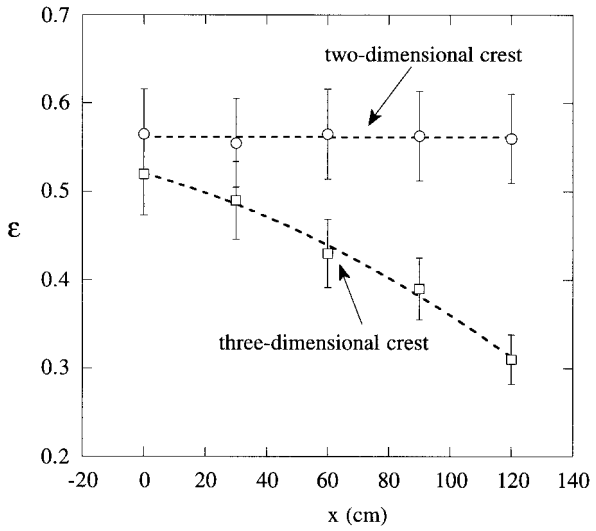

FIG. 7. The crest-front steepness at breaking (see Fig. 5 for definition). The lower steepness as well as the lateral variation in steepness across the three-dimensional breaker suggest the influence of diffraction is to diminish the breaking criteria. Note, for the three-dimensional breaker, $x = 120$ cm marks the edge of the breaking crest.

broke across the entire channel (Fig. 6a). Consistent with previous observations (Bonmarin 1989; Kjeldsen and Myrhaug 1979), both the two- and three-dimensional crests developed front-to-back asymmetry prior to breaking (Fig. 6b), but both the asymmetry and the crest front steepness were greater for the two-dimensional crest, which broke at a steepness $\varepsilon = 0.56$. In contrast, $\varepsilon = 0.52$ at the centerline of the three-dimensional crest and diminished monotonically to $\varepsilon = 0.32$ moving away from the centerline (Fig. 7). For the short-crested wave packet spatial tapering of the input signal created lateral gradients in crest amplitude and thus diffraction. The laterally diminishing breaking steepness was attributed to the influence of diffraction. Complementary to these observations, spatial focusing of wave energy has been observed to increase local breaking steepness. She et al. (1994) examined energy focusing angles from zero, a two-dimensional wave, to 90 degrees and found that the crest front steepness increased monotonically across this range from $\varepsilon = 0.51$ to $\varepsilon = 1.02$. Combining the observations of both studies documents a consistent relationship between breaking steepness and wave field directionality, that is, over a range of conditions spanning negative focusing (diffraction) through zero angle of focus (two-dimensional wave crest) to strongly positive focusing, local steepness at breaking monotonically increases.

We now consider how these observations fit into the paradigm of wave breaking based on crest particle velocity. In the superposition of two, single-frequency, wave trains, that is, crossed waves, the ratio of crest particle velocity to phase velocity is diminished relative to a planar wave of comparable wave amplitude for any angle of crossing (Le Mehaute 1986). This suggests that breaking height should increase as the angle of wave crossing increases. This tendency was confirmed by the experiments of Kolaini and Tulin (1995). In addition, the observations of She et al. (1994) suggest that this result may be extended to focusing wave fields comprised of both multiple interaction angles as well as multiple frequencies. The observations made in the present study, that is, diminished breaking steepness with increasing diffraction, suggest that within diffracting wave packets the ratio of crest particle velocity to phase velocity is increased. To the authors knowledge, no analytical results exist to support this interpretation.

It is also instructive to note the relative timing of breaking onset along the breaking crest. For the two-dimensional breaking condition, breaking was initiated synchronously along the crest. In contrast, along the crescent-shaped crest of the three-dimensional wave, breaking was initiated at the centerline first, and propagated outward, consistent with observations of breaking made in the field. This sequence of breaking, that is, initiation at the centerline and propagation outward, could suggest that breaking at the centerline provokes breaking away from the centerline at less than critical steepness, perhaps through the introduction of turbulence and/or surface instabilities. Consistent with this, previous studies have noted that the steepness required for breaking was lowered by the presence of turbulence left by preceding breaking events (Ramberg and Griffin 1987; Kolaini and Tulin 1995). This suggests that oceanic turbulence generated by wind may encourage breaking below critical conditions described by theory or observed in pristine tank experiments. In addition, once breaking begins the breaking criteria may shift to allow continued breaking at lower steepnesses.

Finally, the steepness values observed along the three-dimensional wave crest fall within the range of steepnesses observed in the field, $\varepsilon = [0.32$ to $0.78]$ (Kjeldsen and Myrhaug 1979), suggesting that field variability may be attributed to variability along individual wave crests. In addition, if one includes the steepness values observed under conditions of wave focusing $\varepsilon = [0.51–1.02]$, from She et al. (1994) and Kolaini and Tulin (1995), the entire range of field variability may be attributed to wave directionality. In fact, the dependence on wave directionality may explain why single point characterizations of wave shape have not been able to provide stable limits for oceanic wave breaking.

b. Spectrum-based wave steepness

The spectrum-based definition of steepness, ak_c, more broadly reflects the spectral content of the wave field. Based on experiments in a wave channel, that is, for two-dimensional wave crests, ak_c proved to be a robust predictor of three distinct breaking conditions: $ak_c = 0.25$ (incipient), $=0.30$ (spiller), and $=0.39$ (plunger)

(Rapp and Melville 1990). For the two-dimensional wave packets considered in this study the following limits were observed: $ak_c = 0.32$ (incipient), 0.38 (spiller), and 0.50 (plunger). The difference in transition criteria observed here and in Rapp and Melville (1990) is attributed to differences in spectral shape, that is, constant component steepness versus constant component amplitude, respectively. The former spectrum is weighted more heavily at the low-frequency end of the frequency band. Chaplin (1996) also considered both of these spectral forms and found an incipient breaking criteria of $ak_c = 0.26$ and 0.30, for the constant amplitude and constant steepness spectra, respectively. Despite a slightly larger bandwidth, $\Delta f/f_c = 0.83$, the upward shift in breaking criteria with increasing weight on lower-frequency components is consistent with the observations made here.

The shift in breaking criteria cannot be attributed to changes in total wave energy. Assuming the same characteristic steepness, the spectral shape $a_n \sim k_n^{-1}$ contains greater total energy than the spectral shape $a_n = \text{const}$. Thus, based on total energy considerations one would expect the constant ak spectra to produce breaking at a lower value of ak_c, but the opposite is true, suggesting that the distribution of spectral energy plays a significant role in defining the breaking point. In particular, observations presented here and by Chaplin (1996) suggest that wave fields consisting of a relatively greater contribution of low-frequency energy are more stable, that is, have higher threshold for breaking. This suggests that the breaking criteria in the field may shift as the wave-field spectrum develops under changing wind conditions.

The breaking criteria also differed between two- and three-dimensional wave packets of the same spectral shape, $a_n \sim 1/k_n$. Note that for the three-dimensional packets the spectral steepness was defined based on the component amplitudes at the centerline. For the short-crested wave packet the transition to each breaking regime occurred at a higher value of ak_c: 0.35 (incipient), 0.39 (spiller), and 0.54 (plunger). The upshift in transition criteria relative to the spectrally similar, two-dimensional packets was attributed to diffraction, which drains energy from the centerline of the short-crested packet even as it evolves to the point of breaking.

The influence of diffraction on the breaking steepness ak_c was explored by varying the parameter y_b/L_0 (Fig. 8). Note that the impact of diffraction on crest development increases with increasing y_b/L_0. For a two-dimensional wave $L_0 \to \infty$ and $y_b/L_0 = 0$ for all values of y_b, suggesting that the evolution of two-dimensional packets are insensitive to y_b. This was demonstrated by Rapp and Melville (1990) who showed that breaking onset as well as energy loss were insensitive to changes in y_b (x_b in RM). A similar result was found here; that is, breaking onset as described by ak_c was independent of y_b for two-dimensional crests.

For the short-crested breakers, the incipient breaking criteria increased monotonically with increasing y_b/L_0 (Fig. 8). An identical trend was observed for the spilling and plunging criteria as well. These observations demonstrate how strongly the global breaking criteria ak_c is influenced by diffraction. Since the global parameter, ak_c, reflects the total energy within the wave spectrum, these observations suggest that more wave energy is needed within a diverging wave field in order to initiate breaking; the corollary of which is that breaking may be suppressed if a wave field is diverging strongly enough. By extrapolation, breaking is encourage in a focused wave field. Because of the strong influence of directionality on breaking criteria, one should use caution when extrapolating two-dimensional laboratory results to three-dimensional wave fields.

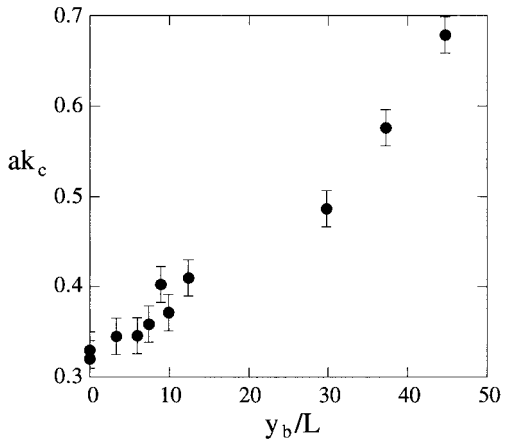

FIG. 8. A breaking criteria based on global steepness, ak_c, increases as the influence of diffraction increases, y_b/L_0. The experiments considered a range of conditions: $L_0 = (30, 60, \text{and } 90 \text{ cm})$ and $y_b = (4, 5, 6)$. Identical trends in steepness were observed for the onset criteria of spilling and plunging.

c. Spectral evolution

As the wave crest approached breaking, the wave profile became sharper and more asymmetric. These changes are reflected in the surface displacement spectra by the appearance of higher harmonics (Tulin and Li 1992). Figures 9, 10, and 11 compare the spectral evolution along the centerline of a short-crested (3D) incipient and plunging wave, and a two-dimensional plunging wave, respectively. The frequency f[Hz] is normalized by the central frequency f_c of the input spectra, and the spectral density $S_{\eta\eta}$ [cm^2 s] is normalized by $k_c^2 f_c$. In each graph the solid line represents the spectrum measured at $y = 0$. The dashed lines represent the spectrum at two downstream positions, $y = 80$ cm ($yk_c = 3.8$) in panels a and $y = 180$ cm ($yk_c = 8.5$) in panels b. The points $y = 80$ and 180 cm are chosen because they depict the most extreme shifts in energy relative to the initial condition. Although the surface displacement at $y = 80$ and 180 cm were measured during separate runs, Fig. 4 confirms that the wave condition,

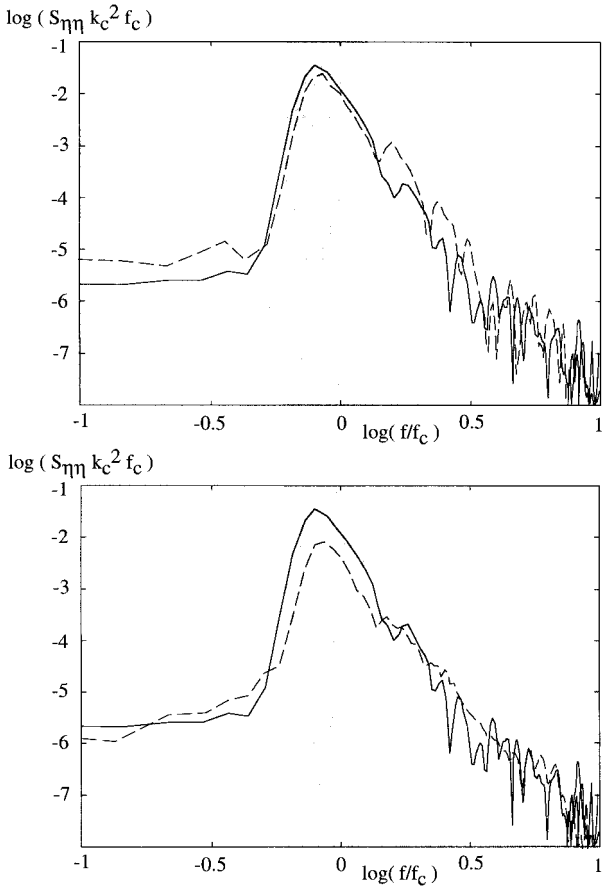

FIG. 9. Surface displacement spectra measured at the centerline of the short-crested, incipient wave packet. In each graph the solid line represents the spectrum measured at y = 0. The dashed lines represent the spectrum at (a: top) y = 80 cm, and (b: bottom) y = 180 cm. The principal and second harmonic bands are shaded in dark and light gray, respectively. The 95% confidence interval for the spectral estimates is equal to 1/2 unit (1/2 decade) on the left axis.

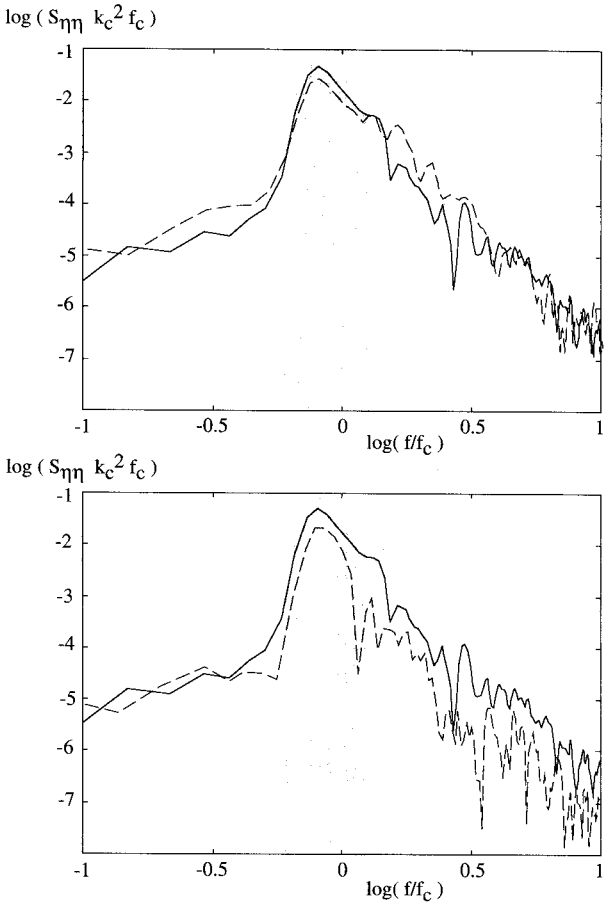

FIG. 10. Same as in Fig. 9 but for the short-crested plunging wave.

as recorded at the reference wave gauge, was identical. Finally, the input and higher frequency bands are shaded in dark and light gray, respectively.

The short-crested incipient wave spectra demonstrates the signature of intrawave energy transfer. Between y = 0 cm and y = 80 cm, the spectral energy within the higher frequency band increases (Fig. 9a) at the expense of the first harmonic band. Similar up-frequency shifts have been observed for focusing wave packets of different spectral shape (Rapp and Melville 1990; She et al. 1994). In addition, the up-frequency energy transfer, associated with the emergence of nonlinear behavior has been explored theoretically and numerically for unifrequency wave trains by McLean (1982). Thus, a similar signature has been observed for four different spectral shapes including both two-dimensional and, in this study, three-dimensional wave evolution.

Beyond the focusing point the energy content of the second frequency band, E_2, returns to its initial level (Fig. 9b), suggesting that the nonlinear interaction producing the up-frequency shift in energy is completely reversible. The reversibility of nonlinear wave–wave interactions was also noted by Rapp and Melville (1990) and by Baldock et al. (1996) who documented both spatial and temporal wave signal symmetry about a focal point for nonbreaking, two-dimensional wave packets. In contrast to the reversible evolution of E_2, the energy of the first harmonic band is not recovered after the focusing event, but exhibits a monotonic decrease. Since no breaking has occurred the steady loss is attributed to diffraction. Diffraction may also affect E_2 with losses proportional to those in E_1; that is, $\Delta E_2 \sim (ak)^2 \Delta E_1$. Using the spectra steepness, $ak_c = 0.35$, the drop in E_2 attributable to diffraction would be 1%, which represents 50% of the observed change, suggesting that diffraction may be important. However, the cycle of increasing and decreasing energy within the higher harmonic band is the same as that observed for a two-dimensional wave that would not be affected by diffraction (Rapp and Melville 1990; Baldock 1996). Thus, it remains unclear how diffraction and frequency focusing interplay.

The incipient wave spectra also indicates an increase in spectral energy below the peak frequency as the wave

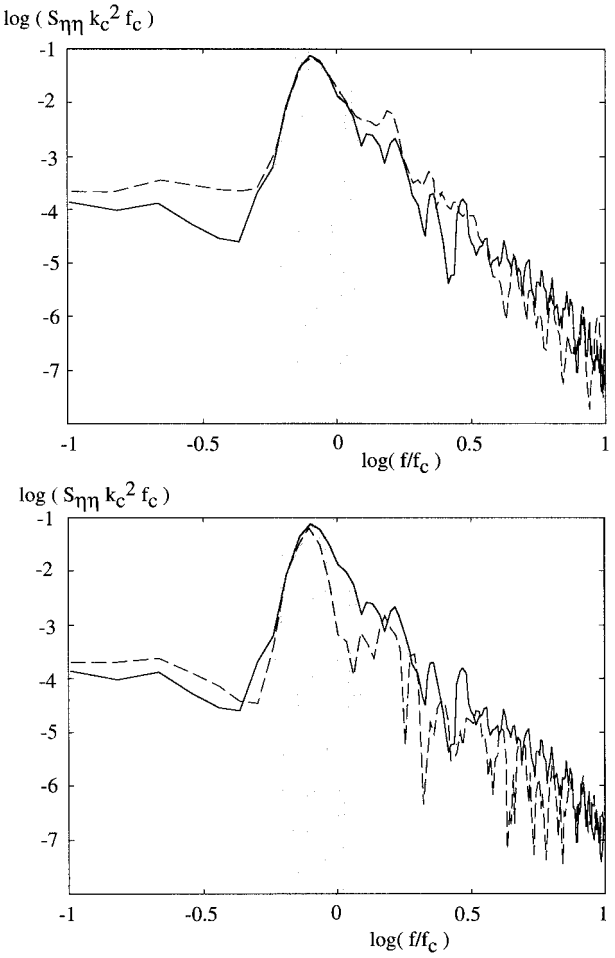

FIG. 11. Same as in Fig. 9 but for the two-dimensional plunging wave.

packet approaches the focal point. This reflects the generation of a forced wave (Fig. 9a). That the low-frequency signature is not apparent at the downstream station ($y = 180$ cm, Fig. 9b) indicated that the forced wave does not leave the test section within the time considered. A similar evolution was observed for two-dimensional incipient waves (Rapp and Melville 1990).

Up to the point of breaking the short-crested plunger evolves in parallel with the incipient wave packet (Figs. 9a and 10a). Specifically, E_2 increases while E_1 is diminished due to diffraction and up-frequency transfer. Growth of the forced wave is also weakly apparent in the lower frequencies. Beyond the focal point the plunger and incipient spectra diverge, with the plunger losing energy from both the first and second frequency bands. As with the incipient wave there is no expression of long wave or mean current energy in the low frequencies at the downstream station (Fig. 10b). This provides additional support for the assumption that within the time interval considered for analysis, mean currents generated by the breaking event do not pass the end of the test section.

To decipher the distribution of losses further, we consider the two-dimensional plunger. The two-dimensional plunger displays the same evolution in E_2, that is, an increase in energy density approaching the point of breaking and subsequent loss of this energy in the process of breaking (Fig. 11). The losses appear in the higher-frequency end of the first frequency band and in the second frequency band. Despite differences in the initial spectral shape, a similar distribution of breaking losses was reported in Rapp and Melville (1990), that is, breaking losses were taken from the higher-frequency end of the spectrum. Within the principle frequency band no losses occur below the peak frequency for the two-dimensional plunger (Fig. 11a). Comparison of the long- and short-crested plungers then suggests that losses below the peak frequency observed in the short-crested wave packet were due to diffraction alone.

The above observations document the signature of frequency focusing and breaking within the evolving surface displacement spectra. Of most interest is the evolution of E_2, which displays nearly identical signatures for both two- and three-dimensional waves. This can be more clearly demonstrated by isolating the evolution of E_2. Figure 12 depicts this evolution at three lateral positions ($x = 0$, 30, and 60 cm) and for conditions of incipient breaking, spilling, short-crested plunging, and two-dimensional plunging. The abscissa depicts the entire test section length, which includes two focal points, $yk_c = 3.8$ and $yk_c = 10.2$, at which the plunger and spiller occurred, respectively. As described previously, within a given wave packet the plunging breaker occurred one wave crest upstream of where the spilling breaker occurred under weaker wave conditions.

The incipient wave condition clearly reflects the two focusing positions. At each focusing position there is an increase in the second frequency band as the wave packet focuses and a subsequent decrease as the wave packet disperses. After each focusing event the energy of the higher-frequency band returns to its initial value, indicating periodic variation but no net loss. This pattern is repeated at each lateral position.

The spilling wave packet passes through the first focusing point ($yk_c = 3.8$) as an incipient wave, and then breaks (spilling) at the second focal point. This evolution is reflected in E_2. At the first focal point the wave spectra evolves in parallel to the incipient wave discussed above, whereas at the second focal point a net loss of energy results from the breaking. The net loss of energy diminishes moving away from the centerline, in particular between gauges 2 and 3 positioned at $x = 30$ and 60 cm, respectively.

The two- and three-dimensional plunging breakers are identical at both gauges 1 and 2, where the short-crested breaker was strongly plunging. In both cases the evolution of E_2 follows the incipient case up to the first focusing peak and then drops sharply, indicating the

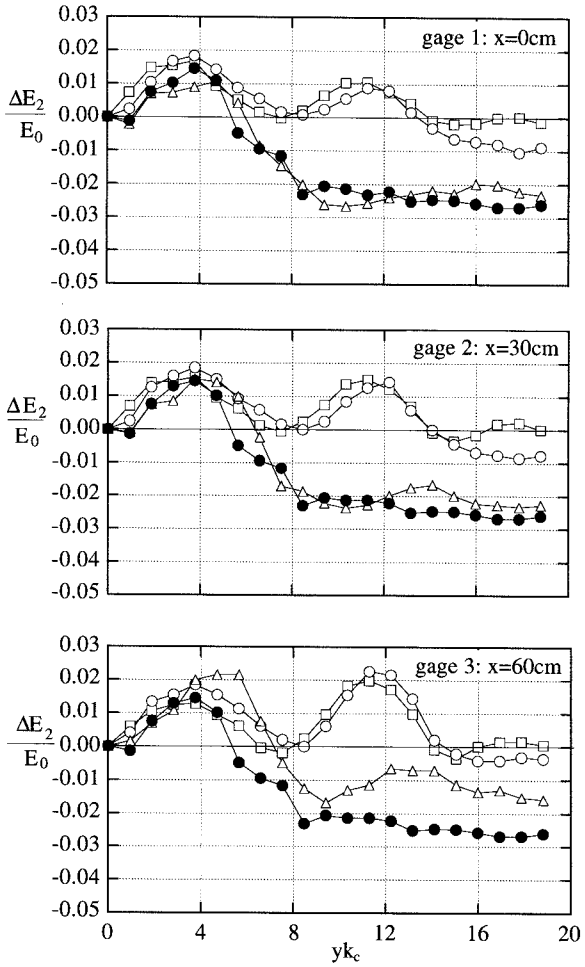

FIG. 12. Evolution of the second harmonic band for a short-crested incipient wave (open squares); a short-crested spilling wave (open circles); a short-crested plunging wave (open triangles); and a two-dimensional plunging wave (closed circles). The three graphs represent observations made at the centerline (a); $x = 30$ cm (b); and $x = 60$ cm (c). Here ΔE_2 represents the change in energy contained in the second harmonic frequency band; E_0 is the total initial wave energy within the wave packet.

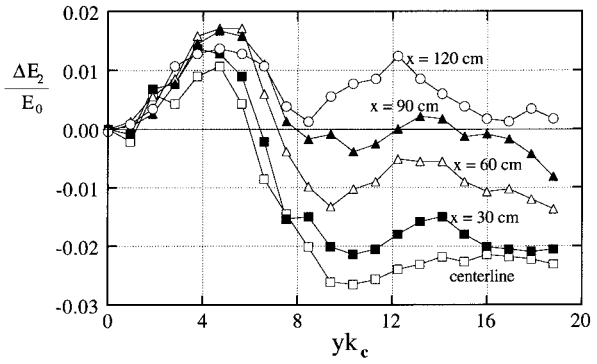

FIG. 13. Evolution of the second harmonic band for the short-crested plunging wave packet. Variation across the wave crest is captured by five lateral positions: (open squares) centerline, (closed squares) $x = 30$ cm, (open triangles) $x = 60$ cm, (closed triangles) $x = 90$ cm, and (open circles) $x = 120$ cm.

breaking losses. At gauge 3 the breaking loss observed for the short-crested breaker is diminished relative to the laterally uniform breaker. This reflects the lateral variation in breaking intensity across the three-dimensional crest. Moving away from the centerline, losses from the three-dimensional plunger diminish and the signature evolves from a plunging wave ($x = 0$, 30 cm), to a spilling wave ($x = 90$ cm), and finally to a nonbreaking, incipient wave ($x = 120$ cm) (Fig. 13). The transitions between wave types suggested by the differences in E_2 evolution are consistent with photographic observations, an example of which is shown in Fig. 14. This suggests that higher harmonic evolution will provide a more robust indicator of breaking that is not influenced by wave directionality, as are both ε and ak_c. Finally, note that even when breaking occurs at the first focal point, the second focal point is expressed in E_2. However, the second focus becomes less distinct and is shifted farther downstream as the breaking intensity increases, that is, closer to the centerline of the breaker (Fig. 13). These shifts suggest that the breaking event alters the subsequent wave evolution.

d. Energy loss

Following the procedure described in section 2e, the breaking losses is computed from the longitudinal variation in $\overline{\eta^2}$ (Fig. 15). In contrast to section 3c, $\overline{\eta^2}$ is now evaluated in a lateral averaged sense to eliminate the local effects of diffraction. The incipient wave indicates a nearly steady decline in wave energy (dashed) that results in a total loss of 6%, attributable to boundary layer losses (Fig. 15a). The predicted frictional loss (dot-dashed) for a laminar boundary layers is 3.6% (Hunt 1952). That the actual loss exceeds the predicted value is attributed to errors associated with the lateral integration of wave energy and with the neglect of higher-order terms.

The variance of both breaking waves follows the same decay up to $yk_c = 2.8$. At this point, about one-half wavelength upstream of breaking onset, the variance begins a steady decline, reflecting the conversion of wave potential energy to wave kinetic energy as the wave steepens (Rapp and Melville 1990). When the wave breaks this energy is lost and the variance does not return to the prebreaking value. The temporary rise in variance observed near $yk_c = 12$ reflects an oscillation in carrier wave steepness arising from wave packet evolution that affects the ratio of kinetic and potential energy. Similar oscillations were observed by Rapp and Melville (1990) in the postbreaking evolution of a two-dimensional wave packet. Within two carrier wavelengths the wave packet variance settles back to a nearly constant but reduced level.

Using the incipient case to delimit frictional losses,

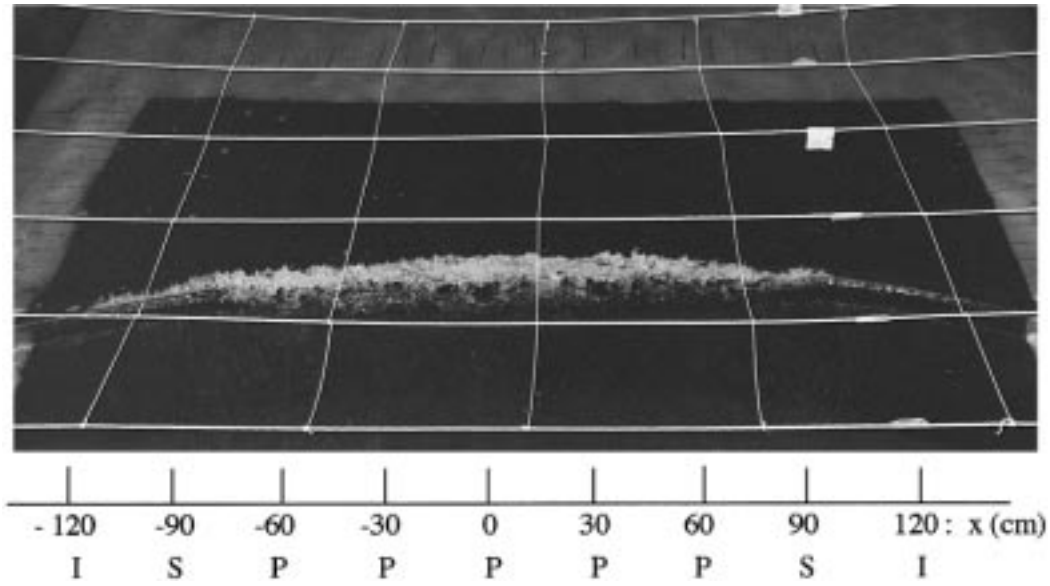

FIG. 14. Photograph of the breaking crest taken from behind the wave; that is, the crest is moving away from the camera. The rope grid (white lines) is positioned 30 cm above the still water surface and is used to determine the wave position and dimensions. The grid boxes are 50 cm × 50 cm. Because of limitations in positioning the camera, the line of sight is offset from the centerline. Using geometry to correct for parallax, the lateral position along the crest line are indicated across the bottom of the image.

the loss due to breaking alone may be estimated as the difference between the breaking and incipient cases (Fig. 15b). The two-dimensional plunger, $ak_c = 0.50$, loses 22 ± 1% of its initial energy to breaking. For a slightly higher steepness, $ak_c = 0.54$, the three-dimensional plunger incurs a laterally averaged loss of 10 ± 1%. This value, however, underestimates the intensity of the short-crested breaker because the lateral average includes crest length that is not breaking. A better comparison is made if the loss due to breaking is normalized only by the energy contained in the breaking crest at the onset to breaking. For the two-dimensional plunger the energy in the crest just prior to breaking is the same as the input energy, excluding viscous losses, and the breaking crest spans the entire test section, so the fractional loss reported above is appropriate. For the three-dimensional plunger the breaking crest is 2.2 ± 0.2 m, including the plunging and spilling regions, based on photographs and the evolution of higher-frequency energy E_2 (Fig. 13). Using the wave energy recorded at $y = 80$ cm to define the energy available in the breaking crest at the onset to breaking, the fractional loss of crest energy during breaking is 16 ± 1%. A smaller loss associated with the three-dimensional plunger is attributed to the fact that the breaking crest includes both plunging and spilling sections. Consistent with this, a 16% loss falls between the losses associated with two-dimensional spilling (10%) and plunging (25%) observed by Rapp and Melville (1990). The trend toward diminished breaking steepness (§3a) along with the diminished breaking severity with decreasing wave focus (conditions of diffraction) complements the observation of increasing breaking steepness and severity with increasing wave focus (She et al. 1994). These observations point out the importance of wave directionality in determining both the onset and severity of breaking events.

4. Summary

Combining observations from the present study with those of She et al. (1994) and Kolaini and Tulin (1995), we confirm that wave directionality affects both the onset and severity of breaking events. As wave directionality varies from negative focusing (diffraction) through planar wave crests to positive focusing, both the breaking crest-front steepness and the breaking severity increase monotonically. In addition, the range of limiting steepness ε observed between conditions of focusing and diffraction cover the range of observations made in the field (Kjeldsen and Myrhaug 1979), suggesting that field variability may be attributed to wave directionality.

The global, spectrum-based wave steepness ak_c is more robust than local wave shape parameters, but is also sensitive to wave-field directionality. In this study the limiting value for ak_c increased by a factor of 2 over a parameter range of $y_b/L_0 = 0$ to 50. While it is difficult to translate the experimental parameter, y_b/L_0, into a field parameter, the trend clearly suggests that ak_c will increase steadily with increasing angle of wave field divergence and that the onset of breaking may be delayed or even suppressed within a diverging wave field.

Finally, within the range of conditions considered in the present study, the effect of wave diffraction was

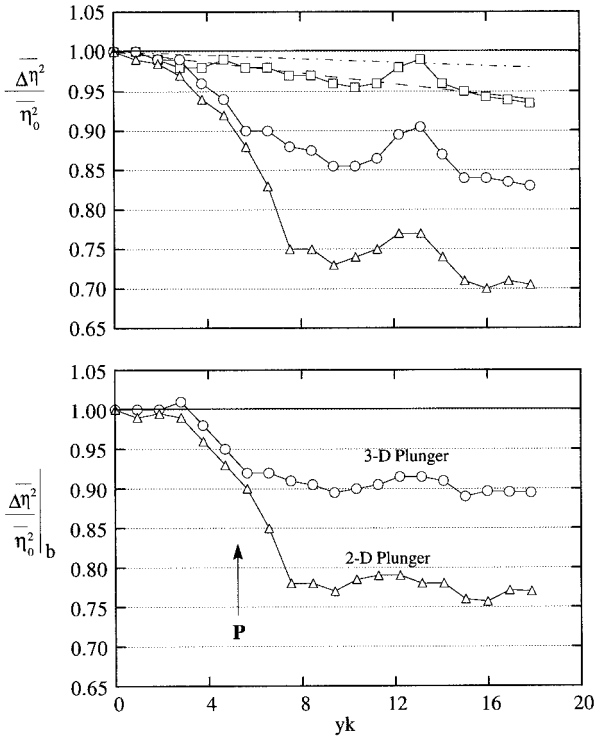

FIG. 15. (a: top) Longitudinal variation in laterally averaged wave packet energy. The lateral average is applied to eliminate the local effects of diffraction. The incipient wave (squares) indicates a nearly steady decline (dashed) that results in a total loss of 6%. The predicted boundary layer loss (dot-dashed) is 2.6%. The short-crested plunger (circles) and two-dimensional plunger (triangles) are also depicted. (b: bottom) Using the incipient case to characterize frictional losses, the loss due to breaking alone may be computed as the difference between the breaking and incipient cases. The resulting variation in wave energy for both the short-crested (circles) and two-dimensional plunger (triangles) is plotted.

only manifest strongly within the principal harmonics, such that the evolution of the higher harmonic bands were identical for two- and three-dimensional waves. In particular, an up-frequency energy shift marked the emergence of nonlinear behavior as the wave packet began to focus longitudinally. Beyond the focal point the up-frequency transfer was completely reversed, unless the wave broke, in which case the up-shifted energy was lost from the wave field. It is interesting to note that the lowest-frequency components did not contribute to the intrawave energy transfer or to the subsequent loss of wave energy that occurred during breaking. In addition, shifts in the breaking criteria ak_c observed with changes in spectral shape suggest that instability and breaking are promoted when a relatively greater contribution of wave energy resides in the higher frequencies (§3b, and Chaplin 1996). Together, the above observations suggest that the breaking process is largely controlled by the evolution of higher-frequency components. Thus, the evolution of a wave field parallels the evolution of a single-frequency wave train for which the development of higher-frequency components, in the form subwavelength modulations, is a precursor to breaking. The above discussions suggest that a breaking criteria based on the evolution of high-frequency components may be a more robust indicator for field application as it is insensitive to wave-field directionality.

Acknowledgments. Support for this work has been provided by ONR Contract N00014-94-1-0610. We also thank Ziad Zakharia for his assistance with the experimental work, and Ole Madsen and Chiang Mei for their helpful editorial comments.

REFERENCES

Baldock, T., C. Swan, and P. Taylor, 1996: A laboratory study of nonlinear surface waves on water. *Philos. Trans. Roy. Soc. London,* **452A,** 649–676.

Banner, M., and O. M. Phillips, 1974: On the incipient breaking of small scale waves. *J. Fluid Mech.,* **77,** 825–842.

Benjamin, T., and J. Feir, 1967: The disintegration of wave trains in deep water. *J. Fluid Mech.,* **27,** 373–397.

Blanchard, D., and A. Woodcock, 1980: The production, concentration and vertical distribution of the sea-salt aerosol. *Ann. N.Y. Acad. Sci.,* **338,** 330–347.

Bonmarin, P., 1989: Geometric properties of deep water breaking waves. *J. Fluid Mech.,* **209,** 405–433.

Bryan, K., and M. Spelman, 1985: The ocean's response to a CO_2-induced warming. *J. Geophys. Res.,* **90,** 11 678–11 688.

Chan, E. S., and W. K. Melville, 1988: Deep water plunging wave pressure on a vertical plane wall. *Proc. Roy. Soc. London,* **417A,** 95–131.

Chaplin, J., 1996: On frequency-focusing unidirectional waves. *Int. J. Offshore Polar Eng.,* **6,** 131–137.

Csanady, G., 1990: The role of breaking wavelets in air–sea gas transfer. *J. Geophys. Res.,* **95,** 749–759.

Cummins, W., 1962: The impulse–response function and ship motion. *Schiffstechnik Forschungsh. Schiffbau Schiffsmaschineubau,* **9,** 101–109.

Davis, M., and E. Zarnick, 1964: Testing ship models in transient waves. *Proc. Fifth Symp. on Naval Hydrodynamics,* Washington, DC, Office of Naval Research, 509–540.

Dawson, T H., D. L. Kriebel, and L. A. Wallendorf, 1993: Breaking waves in laboratory-generated JONSWAP seas. *Appl. Ocean Res.,* **13,** 85–93.

Dean, R., and R. Dalrymple, 1984: *Water Wave Mechanics for Engineers and Scientists.* Prentice-Hall, 174–175.

Duncan, J., 1981: An experimental investigation of breaking waves produced by a towed hydrofoil. *Proc. Roy. Soc. London,* **377A,** 331–348.

——, 1983: The breaking and non-breaking wave resistance of a two-dimensional hydrofoil. *J. Fluid Mech.,* **126,** 507–520.

Gargett, A., 1989: Ocean turbulence. *Annu. Rev. Fluid Mech.* **21,** 419–451.

Greenhow, M., and T. Vinje, 1982: A theoretical and experimental study of the capsize of Salter's Duck in extreme waves. *J. Fluid Mech.,* **118,** 221–239.

Havelock, T., 1918: Periodic, irrotational waves of finite height. *Proc. Roy. Soc. London,* **95A,** 38–56.

Hunt, J., 1952: Viscous damping of waves over an inclined bed in a channel of finite width. *Houille Blanche,* **6,** p. 836.

Johnson, B., and R. Cooke, 1979: Bubble populations and spectra in coastal waters: A photographic approach. *J. Geophys. Res.,* **84,** 3761–3766.

Kjeldsen, S. P., and D. Myrhaug, 1980: Wave–wave interactions, current–wave interactions and resulting extreme waves and breaking waves. *Proc. 17th Conf. on Coastal Engineering,* ASCE, Sydney Australia, 2277–2303.

Koga, M., 1982: Bubble entrainment in breaking wind waves. *Tellus,* **34,** 481–498.

Kolaini, A., and M. Tulin, 1995: Laboratory measurements of breaking inception and postbreaking dynamics of steep short-crested waves. *Int. J. Offshore Polar Eng.,* **5,** 212–218.

Le Mehaute, B., 1986: On the highest periodic short-crested wave. *J. Waterway, Port, Coastal Ocean Eng.,* **112,** 320–330.

Loewen, M. R., and W. K. Melville, 1991: Microwave backscatter and acoustic radiation from breaking waves. *J. Fluid Mech.,* **224,** 601–623.

Longuet-Higgins, M. S., 1969: On wave breaking and equilibrium spectrum of wind. *Proc. Roy. Soc. London,* **310A,** 151–159.

——, 1985a: Bifurcation in gravity waves. *J. Fluid Mech.,* **151,** 457–475.

——, 1985b: Accelaration in steep gravity waves. *J. Phys. Oceanogr.,* **15,** 1570–1579.

——, 1986: Eulerian and Lagrangian aspects of surface waves *J. Fluid Mech.,* **173,** 683–707.

McLean, J., 1982: Instabilities of finite-amplitude gravity waves. *J. Fluid Mech.,* **114,** 315–330.

Mei, C. C., 1983: *The Applied Dynamics of Ocean Surface Waves.* Wiley, 387–390.

Melville, W. K., 1982: The instability and breaking of deep-water waves. *J. Fluid Mech.,* **115,** 163–185.

——, 1996: Wave breaking in air–sea interaction. *Annu. Rev. Fluid Mech.,* **28,** 279–321.

——, and R. J. Rapp, 1988: The surface velocity field in steep and breaking waves. *J. Fluid Mech.,* **189,** 1–22.

Michell, J. H., 1893: On the highest waves in water. *Philos. Mag., Ser. 5,* **365,** 430–437.

Mitsuyasu, H., 1985: A note on the momentum transfer from wind waves. *J. Geophys. Res.,* **90,** 3343–3345.

Myrhaug, D., and E. Dahle, 1994: Ship capsize in breaking waves. *Fluid Structure Interaction in Offshore Engineering,* J. K. Chakrabarti, Ed., Computational Mechanics Publication, 43–84.

Ochi, M. K., and C. H. Tasi, 1983: Prediction of occurrence of breaking waves in deep water. *J. Phys. Oceanogr.,* **13,** 1482–1492.

Penney, W., and A. Price, 1952: Part II. Finite periodic stationary gravity waves in a perfect liquid. *Philos. Trans. Roy. Soc. London,* **244A,** 254–284.

Phillips, O. M., 1958: The equilibrium range in spectrum of wind-generated wave. *J. Fluid Mech.,* **4,** 89–99.

——, 1977: *The Dynamics of the Upper Ocean.* Cambridge University Press, 3–4.

Ramberg, S. E., and O. M. Griffin, 1987: Laboratory study of steep and breaking deep water waves. *J. Waterway, Port, Coastal Ocean Eng.,* **113,** 493–507.

Rapp, R. J., and W. K. Melville, 1990: Laboratory measurements of deep water breaking waves. *Philos. Trans. Roy. Soc. London,* **331A,** 735–780.

Rosengaus-Moshinsky, M., 1987: Experimental study of wave-generated bedforms and resulting wave attenuation. Ph.D. thesis, Massachusetts Institute of Technology, 71–94.

She, K., C. Greated, and W. Easson, 1994: Experimental study of three-dimensional wave breaking. *J. Waterway, Port, Coastal Ocean Eng.,* **120,** 20–36.

Snyder, R., L. Smith, and R. Kennedy, 1983: On the formation of whitecaps by a threshold mechanism. Part III: Field experiment and comparison with theory. *J. Phys. Oceanogr.,* **13,** 1505–1518.

Stokes, G., 1880: Supplement to a paper on the theory of oscillatory waves. *Math. Phys. Papers,* **1,** 314–326.

Su, M. Y., 1982: Three-dimensional deep-water waves, Part 1: Experimental measurements of skew and symmetric wave pattern. *J. Fluid Mech.,* **124,** 73–108.

——, and A. Green, 1985: Wave breaking and nonlinear instability coupling. *The Ocean Surface: Wave Breaking, Turbulent Mixing, and Radio Probing,* Y. Toba and H. Mitsuyasu, Eds., Kluwer Academic, 31–38.

——, M. Bergin, P. Marler, and R. Myrick, 1982: Experiment on nonlinear instabilities and evolution of steep gravity-wave trains. *J. Fluid Mech.,* **124,** 45–72.

Taylor, G. I., 1953: An experimental study of standing wave. *Proc. Roy. Soc. London,* **218A,** 44–59.

Thorpe, S., 1993: Energy loss by breaking waves. *J. Phys. Oceanogr.,* **23,** 2498–2502.

——, 1995: Dynamical process of transfer at the sea surface. *Progress in Oceanography,* Vol. 35, Pergamon, 315–352.

Tulin, M. P., and J. Li, 1992: On the breaking of energetic waves. *Int. J. Offshore Polar Eng.* **2,** 46–53.